NRC Publications Archive
Archives des publications du CNRC

Thermal stability of SrFeO3/Al2O3 thin films: transmission electron microscopy study and conductometric sensing response

Wang, Dashan; Tunney, Jim; Du, Xiaomei; Post, Michael; Gauvin, Raynald

This publication could be one of several versions: author's original, accepted manuscript or the publisher's version. / La version de cette publication peut être l'une des suivantes : la version prépublication de l'auteur, la version acceptée du manuscrit ou la version de l'éditeur.
For the publisher's version, please access the DOI link below./ Pour consulter la version de l'éditeur, utilisez le lien DOI ci-dessous.

Publisher's version / Version de l'éditeur:
https://doi.org/10.1063/1.2957073
Journal of Applied Physics, 104, 2, pp. 023530-023536, 2008

NRC Publications Record / Notice d'Archives des publications de CNRC:
https://nrc-publications.canada.ca/eng/view/object/?id=69375db3-8b17-42fe-957d-a990a0a2ef6d
https://publications-cnrc.canada.ca/fra/voir/objet/?id=69375db3-8b17-42fe-957d-a990a0a2ef6d

Access and use of this website and the material on it are subject to the Terms and Conditions set forth at
https://nrc-publications.canada.ca/eng/copyright
READ THESE TERMS AND CONDITIONS CAREFULLY BEFORE USING THIS WEBSITE.

L'accès à ce site Web et l'utilisation de son contenu sont assujettis aux conditions présentées dans le site
https://publications-cnrc.canada.ca/fra/droits
LISEZ CES CONDITIONS ATTENTIVEMENT AVANT D'UTILISER CE SITE WEB.

Questions? Contact the NRC Publications Archive team at
PublicationsArchive-ArchivesPublications@nrc-cnrc.gc.ca. If you wish to email the authors directly, please see the first page of the publication for their contact information.

Vous avez des questions? Nous pouvons vous aider. Pour communiquer directement avec un auteur, consultez la première page de la revue dans laquelle son article a été publié afin de trouver ses coordonnées. Si vous n'arrivez pas à les repérer, communiquez avec nous à PublicationsArchive-ArchivesPublications@nrc-cnrc.gc.ca.

National Research Council Canada | Conseil national de recherches Canada

Canada

Thermal stability of $SrFeO_3/Al_2O_3$ thin films: Transmission electron microscopy study and conductometric sensing response

Dashan Wang,[1,a)] James J. Tunney,[1] Xiaomei Du,[1] Michael L. Post,[1] and Raynald Gauvin[2]

[1]*Institute for Chemical Process and Environmental Technology, National Research Council of Canada, Montreal Road, Ottawa, Ontario K1A 0R6, Canada*

[2]*Department of Mining, Metallurgy and Materials Engineering, McGill University, Montreal, Quebec H3A 2B2, Canada*

(Received 10 April 2008; accepted 16 May 2008; published online 28 July 2008)

The $SrFeO_3/Al_2O_3$ thin film system has been studied using transmission electron microscopy (TEM). The thin films of $SrFeO_3$ were grown by pulsed laser deposition onto single crystal and sintered polycrystalline Al_2O_3 substrates at room temperature (RT) and 700 °C and subjected to annealing for various periods of time at 700–1000 °C. TEM characterization showed that the morphology of the film varied with changes of deposition temperature. Films deposited at RT featured a columnar structure and those deposited at 700 °C showed layers with crystalline grains. The interfacial structures of the films remained unchanged below 700 °C. Interfacial reactions were observed following annealing at 850 °C for 5 h. The phase transformation at the interface was characterized for the film annealed at 1000 °C for 5 h, for which the principal phases were identified as $SrAl_{2-x}Fe_xO_4$ and $SrFe_{12-y}Al_yO_{19}$. Evaluation for thin film conductometric sensing applications indicated that the untreated films deposited at 700 °C onto both single crystal and sintered Al_2O_3 substrates exhibited a *p*-type gas sensor response to oxygen at 500 °C. *© 2008 American Institute of Physics*. [DOI: 10.1063/1.2957073]

I. INTRODUCTION

Perovskites based on the nonstoichiometric family $SrFeO_{2.5+x}$ $(0<x<0.5)$, herein referred to as $SrFeO_3$, display different crystal structures depending on the degree of oxygen stoichiometry.[1–4] The end member phases for these compounds are the orthorhombic brownmillerite form at $x \sim 0$ and cubic or pseudocubic perovskite at $x>0.4$. At intermediate oxygen stoichiometry, phases based on a distorted cubic structure exist; these are tetragonal and orthorhombic structures that possess longer range ordering of the oxygen sublattice.

Early studies have shown that the interrelationships of the structural and thermodynamic properties of the phases in the bulk powder state are a function of temperature and oxygen partial pressure.[3] Phase transformations are identified using differential thermal analysis, thermogravimetric analysis, oxygen titration, and Mössbauer spectroscopy.[2,3,5] The study of the bulk electrical conductivity of the $SrFeO_3$ system showed that the material is a *p*-type semiconductor within a certain range of $\{T, P_{(O_2)}\}$ with the conductivity of $SrFeO_3$ increasing with increasing of $P_{(O_2)}$,[6] suggesting that this physical property can be exploited for a number of technological applications. As a result, perovskites and related oxides have attracted considerable interest. Efforts from researchers have been made on its extensive applications in a number of areas such as materials for catalysis[7] and solid state gas sensors.[7–12]

$SrFeO_3$ materials can be used as thin film gas sensors[3,4,10,11] since the reversible uptake of oxygen at elevated temperatures $(400<T<600\ °C)$ can readily occur and this compositional change is accompanied by significant changes in electrical conductivity which can be monitored as the sensor transduction signal. However, the electrical and gas sensing properties of films of these material types are strongly dependent on the cation and oxygen stoichiometries[11] and film morphology.[13–18] Variations in microstructure and chemical composition of the thin film could result in failure or drifting of the sensor signal response. In some ceramic-based gas sensors the $SrFeO_3$ thin film gas sensors typically have high sensitivity and rapid response to the changes of analyzed gas concentration at around 500 °C. Hence, the $SrFeO_3$ thin films together with the substrate have to withstand such an elevated temperature in order to maintain long term sensor functionality. However, $SrFeO_3$ thin film gas sensors may be unstable at higher operating temperatures. The films may react with the underlying substrate during the deposition process and subsequent thermal treatments.[19–27] Therefore, it is essential to have a full understanding of the effects of deposition conditions on the thin film structures in order to ensure longer term signal reproducibility in sensor design.

In this study, thin films of $SrFeO_3$ have been grown onto single crystal and sintered polycrystalline Al_2O_3 by pulsed laser deposition (PLD) techniques for investigation of interfacial reactions using transmission electron microscopy (TEM). The films have been prepared under different growth conditions and subjected to postdeposition thermal treatments. Sintered Al_2O_3 was chosen as one of the substrates because it is a cost-effective alternate to single crystal alumina. Single crystalline Al_2O_3 has long been used as substrate for the research on the $SrFeO_3$ thin film sensor devices.

[a)]aElectronic mail: dashan.wang@nrc.ca.

 © 2008 American Institute of Physics

Downloaded 01 May 2009 to 132.246.79.102. Redistribution subject to AIP license or copyright; see http://jap.aip.org/jap/copyright.jsp

The study showed that sensing functionality of $SrFeO_3$ is strongly affected by the film morphology, such as grain size, texture structure, thickness and smoothness of the surface of the film, etc.[3,4,10,11,15,17] Unfortunately, there is lack of report for sintered Al_2O_3 as the substrate for $SrFeO_3$ thin film deposition. Investigation of the thermal stability of thin film systems, especially the $SrFeO_3/Al_2O_3$ (sintered Al_2O_3 substrate) system, becomes more significant than the other. Film structures were examined on the thin film systems grown at RT and 700 °C. Characterization of interfacial reaction and phase transformation were realized on samples of the thin film system after additional annealing at 850 and 1000 °C. Analytical TEM, including high resolution imaging, electron diffraction (ED), and energy dispersive spectrometry, was utilized in the characterization steps. In parallel, an evaluation of the conductometric sensing functionality of the films was conducted on those films grown at 700 °C.

II. EXPERIMENTAL PROCEDURE

A single phase $SrFeO_3$ pellet was used as a target for PLD. $SrFeO_3$ thin films were deposited using the PLD method with a Lambda Physik LPX305i, $\lambda=248$ nm KrF excimer laser. Single crystal $(1\bar{1}02)$ alumina and sintered polycrystalline alumina were used as the substrates with a size of 1×1 cm^2. Films were grown at RT and 700 °C at a laser pulse rate of 8 Hz and pulse duration of about 25 ns under a background oxygen pressure of 100 mTorr. Other experimental details can be found elsewhere.[3,28] Thin film systems were annealed at 700 °C for longer time periods and higher temperatures, i.e., 850 and 1000 °C in air for the study of interfacial reactions. Both cross section and plan view specimens were prepared for TEM examination.[29,30] Cross section specimens are particularly useful for TEM since imaging parallel to the film/substrate interface is possible. The morphology of interfacial reaction products can be revealed in detail. Plan view specimens permit imaging normal to the surface of the film providing a larger field of view. TEM characterization on the thin film systems was realized using a Philips CM20 equipped with an energy dispersive x-ray spectrometer (EDS): INCA Energy TEM 200 and a Gatan UltraScan 1000 charge coupled device camera. The TEM was operated at 200 kV. High resolution imaging and ED techniques in combination with EDS chemical composition analysis were used to investigate the interfacial structure of the film systems.

Electrical conductivity and sensor testing of the $SrFeO_3/Al_2O_3$ film systems was carried out using a two-wire method[4] in a controlled atmosphere environment. Electrical contacts were achieved by thermally depositing 200 nm Au pads directly onto the $SrFeO_3$ films. Sheet resistances and conductivities of the films were calculated from the resistance measurement and corrected for the geometrical configuration of the Au electrode pads and the thickness of the films, which was assumed to be the same for the thin film systems with the two different substrates. The sensing responses of the films as a function of the gas composition were measured isothermally at 500 °C. This was done by measuring the film electrical resistances as the O_2/N_2 gas mixtures were varied from air to oxygen-poor (6% O_2) conditions in a stepwise manner, typically waiting 30 min before changing to the next composition. The gas was then changed in the reverse order from oxygen-poor condition to air in order to verify reversibility. More detailed experimental procedures and conditions can be found elsewhere.[4,10,31]

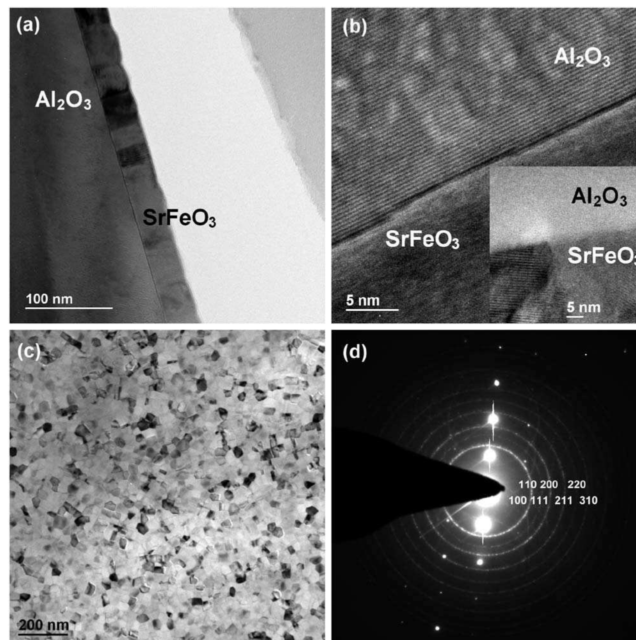

FIG. 1. (a) Cross sectional TEM micrograph of the $SrFeO_3/Al_2O_3$ (sapphire) thin film system deposited at 700 °C for 4 min. (b) HRTEM cross sectional image showing the surface of the Al_2O_3 substrate at the interface and the subgrain film structure (inset). (c) TEM plan view micrograph of the $SrFeO_3$ film. (d) SA ED pattern of the film shown in (c) indicating the phase $SrFeO_{2.97}$.

III. RESULTS AND DISCUSSION

A. As-deposited $SrFeO_3/Al_2O_3$ thin film system

The interfacial structure of $SrFeO_3$ deposited as a thin film onto single crystal Al_2O_3 (sapphire) at 700 °C for 4 min is shown in the TEM images of Fig. 1. The average thickness of the $SrFeO_3$ film is 38 nm and is made up of grains with boundaries that are perpendicular to the substrate. These features are shown in more detail in Fig. 1(a). Each grain contains subgrains that can be identified by contrast difference in a BF image and from the lattice fringes [Fig. 1(b), inset] that indicate the associated orientation and interplanar *d*-spacings. At the interface between $SrFeO_3$ and Al_2O_3, as shown in the high resolution transmission electron microscopy (HRTEM) image in Fig. 1(b), some atomic scaled Al_2O_3 lattice steps are present in a form of surface defect, which implies that no interface interdiffusion reaction has occurred and also that the film has good adhesion to the substrate.

In the image of a plan view specimen shown in Fig. 1(c), the $SrFeO_3$ grain size in the layer is about 40 nm. EDS analysis (not shown) of the film indicates that the elemental composition corresponds to that of the target used in the PLD step, confirming congruent transfer during growth. The SA electron diffraction patterns (EDPs) shown in Fig. 1(d) rep-

Downloaded 01 May 2009 to 132.246.79.102. Redistribution subject to AIP license or copyright; see http://jap.aip.org/jap/copyright.jsp

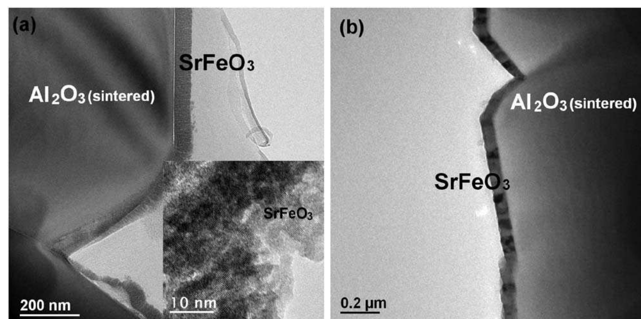

FIG. 2. Cross section TEM micrographs of thin film $SrFeO_3$ deposited onto sintered Al_2O_3 at (a) RT for 4 min where column features and crystallites (inset) are shown and (b) deposited at 700 °C for 4 min where monolayered grains are present.

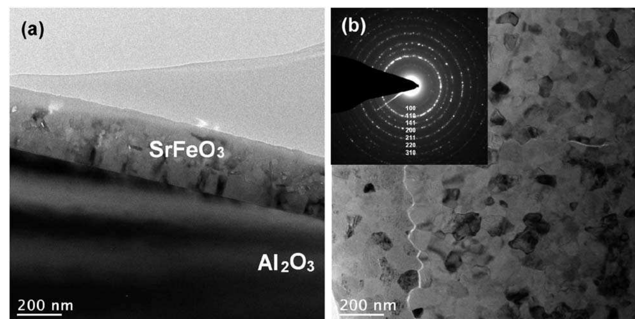

FIG. 3. (a) A cross section image and (b) a plan view image, along with indexed SA diffraction patterns (inset) of the $SrFeO_3$ film deposited at 700 °C for 20 min and annealed in air at 700 °C for 10 h.

resent a combination of reflections from the single crystal Al_2O_3 substrate and the $SrFeO_3$ thin film. The ring patterns were identified as being due to the phase $SrFeO_{2.97}$ (PDF file ID No. 40–0905, cubic $a_0=0.3855$ nm) and are indexed as shown in the figure. Interpretation of the ED patterns shows no evidence of any preferential orientation of the crystalline film.

Structures of $SrFeO_3$ thin films deposited onto a sintered Al_2O_3 substrate at RT and 700 °C for 4 min have also been characterized. The structure of the $SrFeO_3/Al_2O_3$ (sintered) sample deposited at RT for 4 min is shown in the TEM micrograph of a cross section specimen [Fig. 2(a)]. The thickness of the film is 56 nm. The film has a columnar structure with each column consisting of nanoscaled grains, which is also confirmed in the HRTEM image shown as the inset in Fig. 2(a).

Columnar structures are often reported for thin film growth at low temperature. Typically, the overall morphology of the film is dramatically affected by the deposition temperature. Low temperature is in favor of nucleation of the film; however, at low temperature, limited migration or diffusion of the deposited species constrains the crystal growth laterally but facilitates the growth vertically during the deposition. As a result, a fine columnar structure is formed with a high density of crystal defects, pores, and consequent weaker adhesion to the substrate.

X-ray diffraction patterns for these films show low intensity and broadened peaks that could be interpreted as being produced by an amorphous phase. However, the HRTEM image shown in the inset of Fig. 2(a) supports the existence of nanocrystal morphology.

Notches on the surface of the substrate in the cross section image shown in Fig. 2(a) are due to pores that exist at the junctions of the grains of the sintered Al_2O_3. Although the film lies on the substrate along the profile of the surface, gaps between film and substrate are visible as shown in Fig. 2(a), again indicating a poor film adhesion.

Shown in Fig. 2(b) is a cross section of the $SrFeO_3/Al_2O_3$ (sintered) thin film system grown at 700 °C. The thickness of the $SrFeO_3$ film is 60 nm, and it consists of a single row of grains, normal to the substrate and with similar geometry to films deposited onto the single crystalline Al_2O_3 substrate at the same temperature. Also, it is demonstrated by ED that the crystal structure of the $SrFeO_3$ films is identical to that deposited onto single crystal Al_2O_3 under the same conditions. The film in the $SrFeO_3/Al_2O_3$ (sintered) system exhibits an excellent conformation to the rough Al_2O_3 surface, with a uniform film thickness and good adhesion. This is in contrast to $SrFeO_3$ deposited onto sintered Al_2O_3 at room temperature, as shown in Fig. 2(a).

B. Postdeposition thermal treatment of the $SrFeO_3/Al_2O_3$ thin film system

1. Treatment at 700 °C

Films of $SrFeO_3$ deposited onto single crystal and sintered Al_2O_3 substrates at 700 °C for 20 min produce a thicker film (~287 nm) and these have been studied to examine effects due to longer term thermal annealing with subsequent interfacial characterization. These films were annealed at 700 °C for 10 h in air. The interfacial structures of the thin film system [Fig. 3(a)] and the crystal structure [see diffraction pattern shown in the inset of Fig. 3(b)] and chemical composition of the film remain the same as $SrFeO_3$, except for having a larger grain size [Fig. 3(b)], implying that the interfaces of the thin film systems are thermally stable under these conditions.

2. Treatment at 850 °C

Further annealing at higher temperature was conducted in order to investigate the limit of interface thermal stability of the $SrFeO_3/Al_2O_3$ thin film systems. Interfacial reactions began to be observed after additional annealing at 850 °C for 5 h (i.e., 700 °C for 10 h plus 850 °C for 5 h). Shown in Figs. 4(a) and 4(b) are the $SrFeO_3$ thin films on single crystal and sintered Al_2O_3 substrates, respectively, where interfacial reactions have occurred. At the interface, shown in Fig. 4(a), the grains grow into the Al_2O_3 substrate and this penetration results in a fractal shaped boundary. Shown in the inset of Fig. 4(a) is the fractal shaped boundary containing sections of the interface at specific orientations. These sections of interface are believed to be orientated with low interface energy by forming maximum coincident lattice sites shared by both crystalline phases adjacent at the interface. The products of the interfacial reaction are visible in the TEM image [Fig. 4(b)]. The grains adjacent to the film are elongated and oriented along the interface. This region is also identified by EDS as consisting of a new phase or phases due to interfacial

Downloaded 01 May 2009 to 132.246.79.102. Redistribution subject to AIP license or copyright; see http://jap.aip.org/jap/copyright.jsp

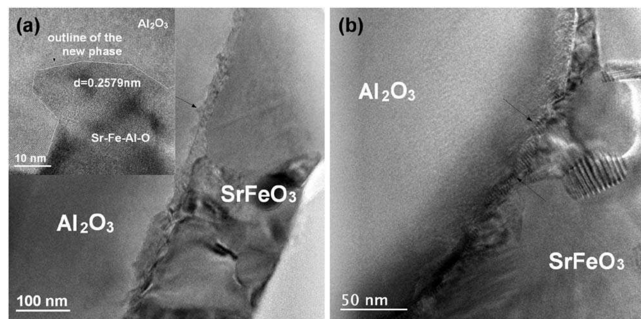

FIG. 4. (a) A cross sectional TEM image of $SrFeO_3/Al_2O_3$ (sapphire) deposited at 700 °C after annealing at 700 °C for 10 h and 850 °C for 5 h, along with a HRTEM image (inset), showing a fractal interface indicated by the arrow. (b) $SrFeO_3/Al_2O_3$ (sintered) film obtained following the same conditions as (a) and showing the interfacial features and new phase formation.

reaction. Since a quantitative analysis was not obtainable on such a limited quantity of material at the interface, conclusive phase identification was not determined. However, EDS analysis showed that the phases contain elemental Al and with $Sr/Fe<1$ compared to $SrFeO_3$. The ED pattern also showed extra weak diffraction rings compared to $SrFeO_3$. Clearly, this is evidence that one or more new phases are forming at the interface at this stage of annealing.

3. Treatment at 1000 °C

Further quantitative identification of the interfacial reaction features was determined on the sample annealed at 1000 °C for 5 h, following prior annealing at 700 °C for 10 h. Shown in Fig. 5(a) is a cross section BF TEM micrograph of this thin film system. The thin film structure consists of a

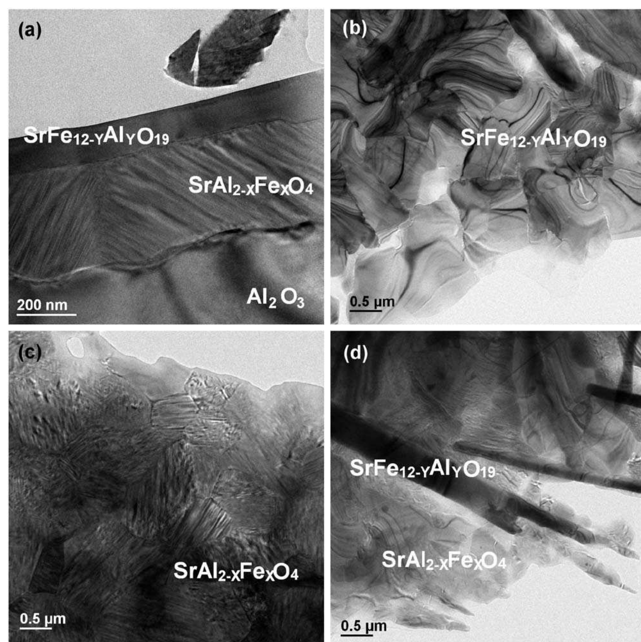

FIG. 5. TEM micrographs of the $SrFeO_3/Al_2O_3$ thin film system deposited at 700 °C for 20 min and annealed at 700 °C for 10 h plus 1000 °C for 5 h. (a) Cross section image of the top and intermediate layer. (b) Plan view image of the top layer. (c) Plan view of the intermediate layer. (d) Plan view image of an area in the top layer showing a mixture of phases from (b) and (c).

top layer and intermediate layer, each with a different morphology that is readily distinguished. The top layer possesses less contrast with uneven thickness ranging from 124 to 160 nm, while the intermediate layer, ranging from 290 to 400 nm in thickness, shows zones filled with bunchlike grains implying a preferential orientation. Individual layers are isolated and the plan view images of the top and intermediate layers are shown in Figs. 5(b) and 5(c), respectively. The grain size for the top layer [Fig. 5(b)] is about the same as the zone size of the intermediate layer shown in Fig. 5(c). The features of the zone in the plan view image are similar to that of a zone shown in the cross section image [Fig. 5(a)], indicating that a zone is formed by stacking a number of parallel-sided slablike grains. Shown in Fig. 5(d) is a plan view of an area in the topmost layer. This shows a mixture of a bar-shaped phase identical to those in the top layer shown in Fig. 5(b) and the zones of the intermediate layer phase as shown in Fig. 5(c). This implies that the intermediate phase has grown and penetrated the film to the outermost surface.

Phase identification in the region of the top layer was realized by applying ED combined with EDS and HRTEM image analysis. The crystallographic information of the phase was obtained using the convergent beam electron diffraction (CBED) technique, and the CBED pattern is shown in Fig. 6(a) along with the zero order Lauer zone (ZOLZ) reflections [inset of Fig. 6(a)]. The first order Laue zone (FOLZ) reflections are present as a high intensity circle. The ZOLZ gives the two-dimensional information about the lattice, and the FOLZ pattern is then used to derive the third dimensional information about the lattice based on the equation[32]

$$R^* \approx (K_t^2 + 2H^*/\lambda)^{1/2}, \tag{1}$$

where K_t is the component of the incident beam and $K_t=0$ when the crystal is in the zone axis orientation, R^* is the radius of a high order Laue zone (HOLZ) reflection ring of the reciprocal lattice, H^* is the height of corresponding HOLZ, and λ is the electron wavelength. Both R^* and H^* are in reciprocal-space units (nm^{-1}).

Symmetry analysis of the CBED pattern shown in Fig. 6(a) gives rise to the possible diffraction groups $6mm1_R$ and $6mm$ for the diffraction pattern, suggesting the type of the crystal system to be hexagonal[33,34] and thus aiding lattice parameter determination. A d-spacing of $d=0.5219$ nm is derived from the ZOLZ reflections, and applying Eq. (1) the interplanar distance along the zone axis is calculated to be $H=2.2902$ nm ($H=1/H^*$). As a result, a hexagonal unit cell is determined for the new phase with $a=0.6027$ nm and $c=2.2902$ nm.

Shown in Fig. 6(b) is a HRTEM image taken from a plan view specimen [Fig. 6(b), left side] along with a filtered image [Fig. 6(b), right side] produced by fast Fourier transform (FFT). The image is a translation of a hexagon with side length $a=0.6034$ nm, which is in agreement with the result derived from the CBED pattern. Since the zone axis of the CBED pattern is parallel to the beam and perpendicular to the thin film surface, this unique orientation relationship makes it suitable for a HRTEM cross section image of the film to acquire supplementary information about the crystal

Downloaded 01 May 2009 to 132.246.79.102. Redistribution subject to AIP license or copyright; see http://jap.aip.org/jap/copyright.jsp

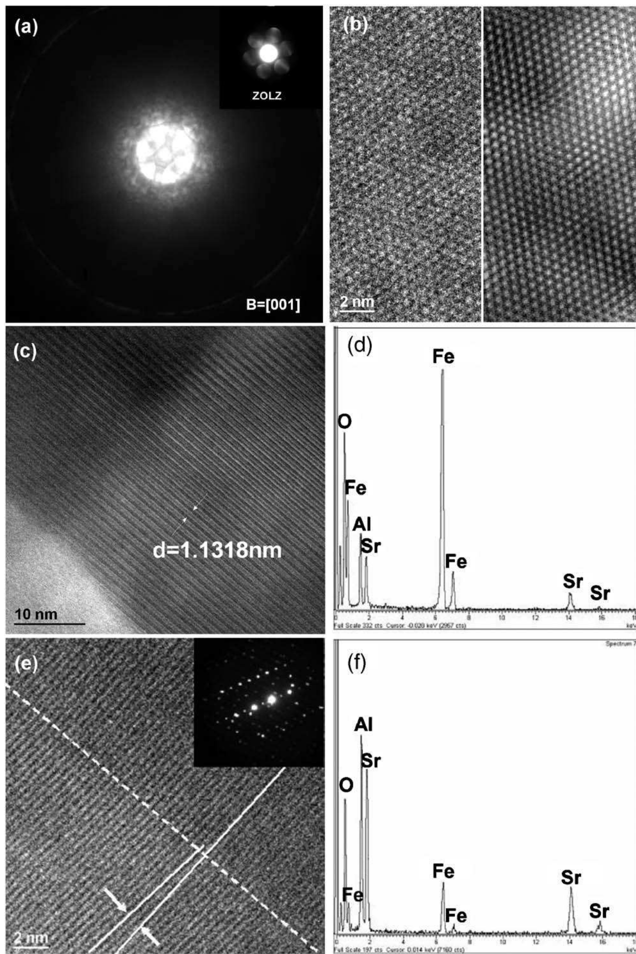

FIG. 6. (a) CBED patterns from the top layer shown in Fig. 5(b) with ZOLZ inset. (b) HRTEM image (left) of the top layer and the FFT filtered image (right). (c) HRTEM cross section image of the top layer, the periodicity of the lattice structure is indicated. (d) EDS spectra from the top layer; Al is present. (e) HRTEM plan view image of the intermediate layer along with a representative EDP, indicating an interfacial relationship in a grain zone and a $SrAl_2O_4$-type crystal structure. (f) EDS spectra of the intermediate layer; Fe is present.

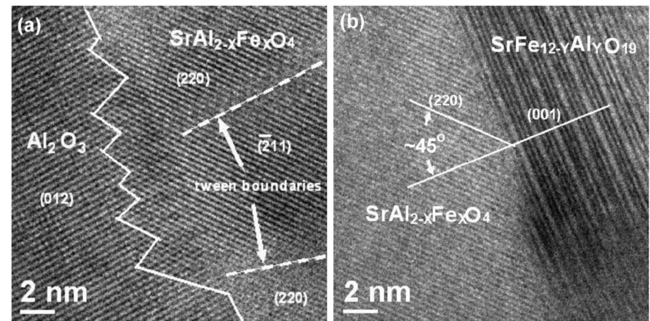

FIG. 7. (a) HRTEM image at the $SrAl_{2-x}Fe_xO_4/Al_2O_3$ interface indicating an irregular geometric interface and crystal orientation relationship. Twin boundaries are arrowed. (b) HRTEM image at the $SrFe_{12-y}Al_yO_{19}/SrAl_{2-x}Fe_xO_4$ interface.

structure. Figure 6(c) is a HRTEM cross section image of the top layer showing a periodicity of an interplanar spacing of 1.1318 nm, which is about half of the measured H from the CBED pattern, supporting the lattice structure determined by CBED. Figure 6(d) is the EDS analysis on the top layer, indicating that the major elemental components in the phase are Fe and O and the minority elements are Sr with a trace of Al. The known material which can best match these data is the phase $SrFe_{12}O_{19}$ (PDF No. 33–1340, hexagonal, $a=0.5886$ nm and $c=2.3037$ nm) with the differences in lattice parameters between the measured and the proposed phase being 2.3% for a and 0.5% for c. This mismatch in parameters may be due to variation in the relative elemental content, which, due to Al being present, is not precisely in the ratio of Sr:Fe:O as 1:12:19. Thus, the compositional formula of the phase is proposed as $SrFe_{12-y}Al_yO_{19}$.

Phase identification for the intermediate layer was realized by microdiffraction on each grain zone. This approach was taken because each zone consists of a number of parallel-sided slablike grains acting as a single crystal with twin boundaries or small-angle grain boundaries as the main crystal defects [Fig. 6(e)]; therefore, a selected area does not contain enough grains to produce an EDP with continuous rings like those shown in Fig. 1(d). A representative EDP from a slablike grain zone is shown in the inset of Fig. 6(e). It is apparent that diffraction streaks have resulted from an array of slabs that are lying inversely to the thickness of the slabs and having a small orientation difference. A series of d-spacings was obtained by taking EDPs from many grain zones, with which the d-spacings of the phase known as $SrAl_2O_4$ (PDF No. 34–0379, monoclinic, $a=0.8442$ nm, $b=0.8822$ nm, and $c=0.5161$ nm) were compared. Thus, the Bravais lattice of the phase is determined to be of the $SrAl_2O_4$ type. However, information from the EDS analysis, shown in Fig. 6(f), indicates that the phase also contains some Fe; therefore the formula of the phase is suggested as $SrAl_{2-x}Fe_xO_4$. The Fe is assumed to substitute for Al from a consideration of matched valency in the compound and the closer ionic radius of Fe^{3+} (0.645 Å) to Al^{3+} (0.535 Å) than to Sr^{2+} (1.12 Å).[35]

The growth front at the evolving interface can be found as shown in Fig. 7(a), which is a HRTEM image of the region between Al_2O_3 and $SrAl_{2-x}Fe_xO_4$. The $Al_2O_3/SrAl_{2-x}Fe_xO_4$ interface is outlined with a fractal line. The phase $SrAl_{2-x}Fe_xO_4$ penetrates the Al_2O_3, suggesting a crystal structure that is evolving from $SrAl_{2-x}Fe_xO_4$ into Al_2O_3 and with specific orientations between the adjacent phases. Shown in Fig. 7(b) is a HRTEM image of the region between $SrAl_{2-x}Fe_xO_4$ and $SrFe_{12-y}Al_yO_{19}$. Unlike the fractal feature of the $Al_2O_3/SrAl_{2-x}Fe_xO_4$ interface, the $SrAl_{2-x}Fe_xO_4/SrFe_{12-y}Al_yO_{19}$ interface consists of parallel sections connected by steps of atom planes, which implies a different growth mechanism of $SrAl_{2-x}Fe_xO_4$ at this interface from that at the $Al_2O_3/SrAl_{2-x}Fe_xO_4$ interface. The phase $SrFe_{12-y}Al_yO_{19}$ is considered to be consumed during the growth of $SrAl_{2-x}Fe_xO_4$.

The orientational relationship between the crystalline $SrAl_{2-x}Fe_xO_4$ growth and the Al_2O_3 substrate is determined by identifying the crystal planes represented by the lattice fringes. The angle between the (220) of $SrAl_{2-x}Fe_xO_4$ and (012) of Al_2O_3 is ~45° as shown in Fig. 7(a). In the region of $SrAl_{2-x}Fe_xO_4$, the parallel-sided slabs are separated by small angled boundaries as shown in Fig. 6(e). The angle

Downloaded 01 May 2009 to 132.246.79.102. Redistribution subject to AIP license or copyright; see http://jap.aip.org/jap/copyright.jsp

between the planes (220) of $SrAl_{2-x}Fe_xO_4$ and (001) of $SrFe_{12-y}Al_yO_{19}$ is also about 45° as shown in Fig. 7(b). This match in lattice geometric orientation is presumably governed by the system minimizing the interface energy.

C. Chemistry of the $SrFeO_3/Al_2O_3$ thin film system at 1000 °C

The chemical reactions driving the phase transformation, as a result of the formation of the new phases, is proposed using the following sequence of equations:

$$6Sr_2Fe_2O_5 = 11SrO + SrFe_{12}O_{19}. \quad (2)$$

Note that $Sr_2Fe_2O_5$ ($2SrFeO_{2.5}$) is used rather than $SrFeO_3$ ($SrFeO_{2.5+x}$) in Eq. (2). This is because the oxygen stoichiometry of $SrFeO_3$ changes with the environmental temperature. At higher temperatures, ordered oxygen atoms in the octahedral positions in the $SrFeO_3$ lattice are labile and are removed from the lattice as gas phase O_2 to leave the $SrFeO_{2.5}$ phase.[4]

Equation (2) describes the fact that at the interface of $Al_2O_3/SrFeO_3$, decomposition of $Sr_2Fe_2O_5$ induced by diffusion of Sr from $Sr_2Fe_2O_5$ results in the formation of the new phase $SrFe_{12}O_{19}$. Accompanying this process, further diffusion of Sr into Al_2O_3 proceeds, as shown in Eq. (3),

$$Al_2O_3 + SrO = SrAl_2O_4. \quad (3)$$

Thus, the additional phase forms, and a new interface structure is created, i.e., $Al_2O_3/SrAl_2O_4/SrFe_{12}O_{19}/SrFeO_3$. For simplicity, diffusions of Fe and Al across the interfaces are not specifically shown in the equations; therefore, $SrAl_2O_4$ and $SrFe_{12}O_{19}$ represent the phases $SrAl_{2-x}Fe_xO_4$ and $SrFe_{12-y}Al_yO_{19}$, respectively, and the overall reaction (4) is given by combining Eqs. (2) and (3),

$$11Al_2O_3 + 6Sr_2Fe_2O_5 = 11SrAl_2O_4 + SrFe_{12}O_{19}. \quad (4)$$

To further define the diffusion aspects of the interfacial reactions, a schematic illustration of the evolving interfacial structure of the $SrFeO_3/Al_2O_3$ thin film system after different thermal treatments is shown in Fig. 8. Figure 8(a) represents the structure of the $SrFeO_3/Al_2O_3$ (sapphire) film system deposited at 700 °C for 20 min and annealed at 700 °C for 10 h, where no interfacial reactions have yet initiated. Figure 8(b) represents the thin film system following additional annealing at 850 °C for 10 h. As a result of this thermal treatment, new phases now precipitate at the $SrFeO_3/Al_2O_3$ interface. Shown in Fig. 8(c) is the schematic structure of the thin film system following an additional anneal of 10 h at 700 °C plus a further 5 h at 1000 °C. Figure 8(c) now indicates the expanded depth of penetration of the new phases, $SrAl_{2-x}Fe_xO_4$ and $SrFe_{12-y}Al_yO_{19}$, as both the Al_2O_3 substrate and the initial $SrFeO_3$ film are consumed.

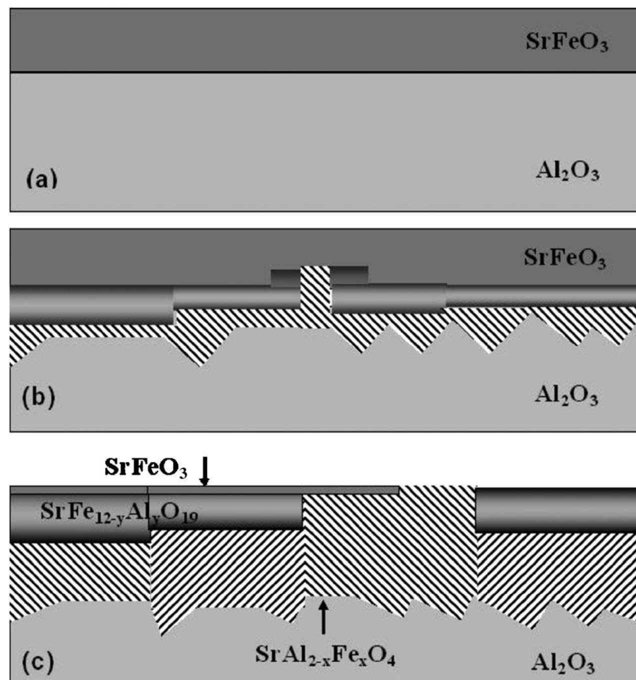

FIG. 8. Schematic illustration of the interface evolution for the $SrFeO_3/Al_2O_3$ thin film system: (a) as deposited at 700 °C and annealed at 700 °C for 10 h, (b) after additional annealing at 850 °C for 10 h, and (c) after further annealing at 1000 °C for 5 h.

D. Conductometric sensor data

$SrFeO_3/Al_2O_3$ (single crystalline and sintered Al_2O_3) obtained at 700 °C were evaluated for thin film conductometric sensing applications because of their good interfacial thermal stability. The results indicate that films deposited onto both single crystal and sintered Al_2O_3 substrates exhibited very similar responses to variations in oxygen concentration at 500 °C (Fig. 9). In both cases, changing the concentration from 20% oxygen to 6% oxygen in balance nitrogen caused the resistance to reversibly increase approximately 30%. This is indicative of the *p*-type semiconductor gas sensor response that it expected for $SrFeO_3$ materials.[6] This similarity of response indicates that it is legitimate to employ $SrFeO_3$ deposited onto single crystalline Al_2O_3 as a model system for $SrFeO_3$ deposited onto sintered Al_2O_3 commercial sensor platforms. No substantial baseline drift was observed after repeated exposures for either of these films, indicating that the interfacial diffusion is negligible at the $T=500$ °C operating temperature for this system.

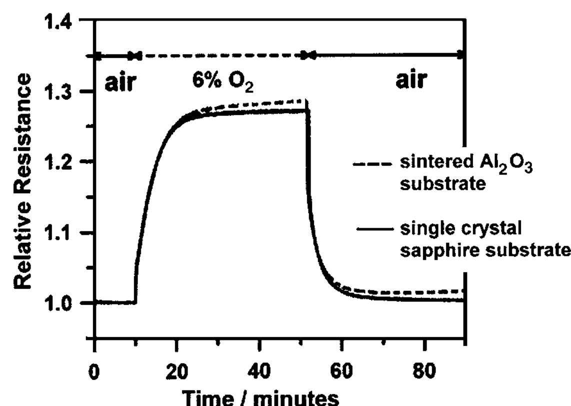

FIG. 9. Temporal electrical resistance response of the $SrFeO_3$ films at 500 °C in air (O_2 concentration 20%) when exposed to a 6% O_2 in $/N_2$ mixture. Response is shown for $SrFeO_3$ on both sapphire and sintered Al_2O_3 substrates.

Downloaded 01 May 2009 to 132.246.79.102. Redistribution subject to AIP license or copyright; see http://jap.aip.org/jap/copyright.jsp

IV. CONCLUSIONS

The films of the nonstoichiometric perovskite grown onto single crystalline and sintered polycrystalline Al_2O_3 substrates by PLD at different temperatures with additional postdeposition thermal treatments have been characterized with TEM for the investigation of interfacial structure and reactions. The interface of the $SrFeO_3$ films deposited onto single crystal and sintered Al_2O_3 substrates remained stable following thermal annealing up to 700 °C for 10 h. Interfacial reactions were observed in the $SrFeO_3/Al_2O_3$ thin film system after annealing at 700 °C for 10 h followed by additional annealing at 850 °C for 5 h.

Phase transformation and reactions were characterized at the interface of the $SrFeO_3/Al_2O_3$ thin film system annealed at 1000 °C. The phases formed at the interface between $SrFeO_3$ and Al_2O_3 were identified as $SrAl_{2-x}Fe_xO_4$ and $SrFe_{12-y}Al_yO_{19}$.

Both systems ($SrFeO_3$ with single crystal and sintered Al_2O_3 substrates) show similar sensor response to oxygen at 500 °C and can be taken as comparable sensor systems. The relative thermochemical stability of the $SrFeO_3/Al_2O_3$ system below $T=700$ °C is reflected by its low baseline drift.

[1] J. P. Hodges, S. Short, J. D. Jorgensen, X. Xiong, B. Dabrowski, S. M. Mini, and C. W. Kimball, J. Solid State Chem. **151**, 190 (2000).
[2] Y. Takeda, K. Kanno, T. Takada, O. Yamamoto, M. Takano, N. Nakayama, and Y. Bando, J. Solid State Chem. **63**, 237 (1986).
[3] M. L. Post, B. W. Sanders, and P. Kennepohl, Sens. Actuators B **13**, 272 (1993).
[4] J. J. Tunney and M. L. Post, J. Electroceram. **5**, 63 (2000).
[5] S. Wiβmann and K. D. Becker, Solid State Ionics **85**, 279 (1996).
[6] J. Hombo, Y. Matsumoto, and T. Kawano, J. Solid State Chem. **84**, 138 (1990).
[7] K. Ichimura, Y. Inoue, I. Yasumori, B. Viswanathan, and T. Arakawa, in *Properties and Applications of Perovskite-Type Oxides*, edited by L. G. Tejuca and J. L. G. Fierro (Marcel Dekker, New York, 1993), pp. 235, 271, 361.
[8] D. E. Williams, in *Solid State Gas Sensors*, edited by P. T. Moseley and B. C. Tofield (The Adam Hilger Series on Sensors, Bristol, Philadelphia, 1987), Chap. 5.
[9] G. Eranna, B. C. Joshi, D. P. Runthala, and R. P. Gupta, Crit. Rev. Solid State Mater. Sci. **29**, 111 (2004).
[10] M. L. Post, J. J. Tunney, D. Yang, X. Du, and D. L. Singleton, Sens. Actuators B **59**, 190 (1999).
[11] J. J. Tunney, M. L. Post, X. Du, and D. Yang, J. Electrochem. Soc. **149**, H113 (2002).
[12] G. Martinelli, M. C. Carotta, M. Ferroni, Y. Sadaoka, and E. Traversa, Sens. Actuators B **55**, 99 (1999).
[13] K. Sahner, R. Moos, M. Matam, J. J. Tunney, and M. L. Post, Sens. Actuators B **108**, 102 (2005).
[14] N. Barsan and U. Weimar, J. Electroceram. **7**, 143 (2001).
[15] C. Xu, J. Tamaki, N. Miura, and N. Yamazoe, Sens. Actuators B **3**, 147 (1991).
[16] D. E. Williams and K. F. E. Pratt, Sens. Actuators B **70**, 214 (2000).
[17] Z. Wang, T. Sasaki, N. Koshizaki, J. J. Tunney, and M. L. Post, Thin Solid Films **437**, 95 (2003).
[18] B. R. Sanders, J. Yao, and M. L. Post, *Polycrystalline Thin Films: Structure, Texture, Properties and Applications*, edited by, K. Barmak, M. A. Parker, J. A. Floro, R. Sinclair, and D. A. Smith Materials Research Society Symposium Proceedings No.343, San Francisco, U.S.A 1994), p.463.
[19] J. J. Tunney, P. Whitfield, X. Du, and M. L. Post, Thin Solid Films **426**, 221 (2003).
[20] R. Moos, F. Rettig, A. Hürland, and C. Plog, Sens. Actuators B **93**, 43 (2003).
[21] S. J. Litzelman, A. Rothschild, and H. L. Tuller, Sens. Actuators B **108**, 231 (2005).
[22] X.F. Chen, H. Lu, W.G. Zhu, and O.K. Tan, Surf. Coat. Technol. **198**, 266 (2005).
[23] S. H. Oh and C.-G. Park, Surf. Interface Anal. **31**, 796 (2001).
[24] X. B. Lu, X. Zhang, R. Huang, H. B. Lu, Z. H. Chen, W. F. Xiang, M. He, B. L. Cheng, H. W. Zhou, X. P. Wang, C. Z. Wang, and B. Y. Nguyen, Appl. Phys. Lett. **84**, 2620 (2004).
[25] X. B. Lu, Z. G. Liu, G. H. Shi, H. Q. Ling, H. W. Zhou, X. P. Wang, and B. Y. Nguyen, Appl. Phys. A: Mater. Sci. Process. **78**, 921 (2004).
[26] J. Q. He, C. L. Jia, V. Vaithyanathan, D. G. Schlom, J. Schubert, A. Gerber, H. H. Kohlstedt, and R. H. Wang, J. Appl. Phys. **97**, 104921 (2005).
[27] D. Wang, J.J. Tunney, X. Du, M.L. Post, and R. Gauvin, J. Mater. Res. **22**, 1, (2007).
[28] B. W. Sanders and M. L. Post, Laser Ablation in Materials Processing: Fundamentals and Applications edited by B. Braren, J. J. Dubowski, and D. P. Norton, (Materials Resarch Society, Pittsburgh PA 1993) Symposium Proceedings Vol. 285, p.427.
[29] P. J. Goodhew, *Specimen Preparation for Transmission Electron Microscopy of Materials* (Oxford University Press, New York, 1984).
[30] D. G. Ivey and G. R. Piercy, J. Electron Microsc. Tech. **8**, 233 (1988).
[31] M. L. Post, J. J. Tunney, and J. Yao, *Chemical and Biological Sensors and Analytical Electrochemical Methods*, The Electrochemical Society Proceedings Series, edited by A. J. Ricco, M. A. Butler, P. Wanysek, G. Horvai, and A. F. Silva (The Electrochemical Society, Inc., Pennington, NJ, 1977), p. 889.
[32] J. C. H. Spence and J. M. Zuo, *Electron Microdiffraction* (Plenum Press, New York, London, 1992), p. 158.
[33] M. H. Loretto, *Electron Beam Analysis of Materials* (Chapman and Hall, London, 1984), p. 88.
[34] B. F. Buxton, J. A. Eades, J. W. Steeds, and G. M. Rackham, Philos. Trans. R. Soc. London, Ser. A **281**, 171 (1976).
[35] Edded by J. A. Dean, *Lange's Handbook of Chemistry*, 15th ed. (McGraw-Hill, New York, 1999), p. 528.

Downloaded 01 May 2009 to 132.246.79.102. Redistribution subject to AIP license or copyright; see http://jap.aip.org/jap/copyright.jsp